Polymer 50 (2009) 3378–3385

Contents lists available at ScienceDirect

Polymer

journal homepage: www.elsevier.com/locate/polymer

Heat transport in epoxy networks: A molecular dynamics study

Vikas Varshney [a,b,*], Soumya S. Patnaik [a], Ajit K. Roy [a], Barry L. Farmer [a]

[a] Materials and Manufacturing Directorate, Air Force Research Laboratory, Wright Patterson AFB, Dayton, OH 45433, USA
[b] Universal Technology Corporation, Dayton, OH 45432, USA

ARTICLE INFO

Article history:
Received 23 February 2009
Received in revised form
13 May 2009
Accepted 14 May 2009
Available online 22 May 2009

Keywords:
Molecular dynamics
Thermal conductivity
Epoxy network

ABSTRACT

In this article, thermal behavior of an epoxy based thermoset polymer has been discussed using atomistic molecular dynamics simulations. The simulations were performed on crosslinked network of EPON-862 and curing agent-W (DETDA) using consistent valence force field (CVFF). Thermal conductivity was calculated using both equilibrium as well as non-equilibrium molecular dynamics approaches and the results were found to be in good agreement with experimental findings. Different contributions of heat flux vector towards thermal conductivity and their possible coupling are discussed in terms of various convective and virial contributions. In addition, discussion of power spectra analysis of velocity auto-correlation function for crosslinked network shows a broad distribution of low frequency vibrational modes suggesting distribution of relaxation times.

1. Introduction

Thermal transport in solid materials is predominantly governed by the phenomenon of heat conduction [1]. As a result, a great amount of research has been done to study this phenomenon in significantly diverse class of materials which include metals, ceramics, alloys, composites, etc. [2]. Among these materials, epoxy resin based thermosets and their composites presents a special class of materials which possess excellent mechanical properties (leading to their widespread use in aerospace and automobile industry [3]). However, they are considered to be poor materials for thermal transport due to their low thermal conductivity [4]. The issue of thermal transport through these epoxy networks becomes quite significant in situations where they are used as adhesive glues to join two thermally conductive materials (for example in space applications), and hence presents a severe bottleneck for the thermal transport [5]. It has also been shown experimentally that even dispersing highly thermally conductive secondary phases, such as CNTs and nano-particles above their percolation threshold limit, does not significantly enhance the thermal conduction properties of these material systems [6]. In order to improve or alter the thermal conduction in these systems, it is important to understand what modes and interactions govern heat transport in network glassy polymers.

The thermal transport in glassy systems, especially the temperature dependence of thermal conductivity has been studied theoretically. Karpov and Parshin [7] modeled amorphous systems based on scattering of anharmonic modes from two-level systems (TLS). In late 80's, Alexander et al. and Jagannathan et al. [8] predicted the linear dependence of thermal conductivity over temperature based on anharmonic interactions between localized (fracton) and non-localized (phonon) vibrational modes. They introduced these interactions as phonon-assisted fracton hopping, which contribute to heat current, generating thermal conductance. Later on in early 90's, Feldman et al. [9] modeled the thermal conductivity of amorphous Si and proposed that harmonic diffusion of thermal energy between delocalized (extended) states dominates the thermal transport and predicted observed temperature dependence of thermal conductivity.

Molecular modeling provides a complimentary route to experiments to study structure–property relationships. Not only it helps in providing a molecular level understanding in a very cost effective manner without performing actual experiments, it also provides a foundation for developing accurate theories and in designing better materials with tailored properties. Molecular dynamics (MD) simulations [10] explore the system properties by assigning interaction parameters to its constituent elements (atoms) whose dynamics is governed by Newtonian equations of motion. To study the material properties of epoxy networks, several groups have employed atomistic [11] as well as coarse-grained [12] molecular dynamics simulations. The literature is however almost entirely focused on studying mechanical and structural properties of these polymers with no reference to their thermal behavior, presumably

* Corresponding author.
E-mail address: vikas.varshney@afmcx.net (V. Varshney).

0032-3861/$ – see front matter © 2009 Elsevier Ltd. All rights reserved.
doi:10.1016/j.polymer.2009.05.027

due to their widely accepted role as structural materials. Given the fact that electronic contribution towards thermal transport in organic polymeric systems is sufficiently low as compared to phononic (vibrational) contribution, MD simulations which treat these vibrations explicitly should be adequate to address the thermal behavior.

Equilibrium MD (EMD) based on Green-Kubo formalism [13] and non-equilibrium MD (NEMD) based on Fourier law formalism [14] are widely used to simulate thermal transport behavior. While EMD simulations are best suited for studying homogenous systems, NEMD simulations have an advantage when studying heterogeneous systems [15]. Although a number of studies have reported using MD simulations to study thermal properties at the molecular level, most of these studies have been performed on ordered systems such as carbon nanotubes [16,17], ionic salts [18], silicon [19] and metals [20], where thermal conductivity can be described by propagation of well separated acoustic phonons through the system. Atomistic simulations based study of thermal behavior of polymeric systems [21,22] are very few.

In this article, we have put forward one of the first attempts to explore the thermal properties of crosslinked polymer system, specifically, epoxy networks, using atomistic molecular dynamics simulations using both EMD and NEMD approaches. In our present simulations, the network polymer is based on EPON-862 epoxy resin and curing agent-W (DETDA) [23]. The motivation for this work is to explore the molecular origins of thermal transport in thermoset polymers. The study is expected to provide an insight into the relationship between structure and thermal properties of thermoset polymers.

The flow of the present article is as follows. In the next section, we have presented our model as well as simulation details along with a brief theoretical background of both NEMD and EMD simulations. Subsequently, we have presented thermal conductivity calculations from NEMD and EMD approaches followed by power spectrum analysis of velocity autocorrelation functions. Thereafter, various convective and virial contributions towards thermal conductivity are briefly discussed. We also compare our simulation results with experimental findings wherever possible. Towards the end, we conclude the article by summarizing important findings of the work.

2. Theoretical background

2.1. Formalism of thermal conductivity based on Fourier law approach (NEMD)

The Fourier law approach is based on the principle of heat conduction which states that under steady-state conditions, amount of heat flow per unit area in unit time is directly proportional to the temperature gradient at the cross-section [24]. This proportionality constant is widely known as thermal conductivity (λ) and is shown in Eq. (1). This method for the calculation of thermal conductivity from molecular dynamics simulations is also known as direct method as it is quite analogous to experimental conditions.

$$\lambda = \frac{Q/A\Delta t}{\mathrm{d}T/\mathrm{d}z} \tag{1}$$

Here, Q is heat flow through the cross-section, A is the cross-sectional area, Δt is the time for which heat is flowing and $\mathrm{d}T/\mathrm{d}z$ is the steady-state temperature gradient. Once, the heat flow and temperature gradient are known from simulation, the thermal conductivity is easily calculated using Eq. (1). A representative protocol for the calculation of $Q/A\Delta t$ and $\mathrm{d}T/\mathrm{d}z$ from molecular dynamics simulations is briefly discussed below.

First of all, the system of interest is built as a thin slab with large aspect ratio along the heat flow direction and is equilibrated at desired temperature and pressure. Next, the central part of the slab is heated to desired high temperature, T_{high} and is kept at that temperature while the end boundaries are cooled to desired low temperature T_{low}. In order to keep the regions at their specified temperatures, energy is continuously added and taken off from hot and cold regions during the course of the simulation, respectively. Energy addition or removal is done in terms of modifying kinetic energy by velocity rescaling procedure in both hot and cold thermostats, respectively. In doing so, a temperature gradient is established across the slab. In order to calculate the temperature gradient, the slab is divided into pre-defined number of small slabs with equal thickness. Thereafter, the temperature of each slab is calculated as follows [24].

$$T_i = \frac{1}{3N_i k_{\mathrm{B}}} \sum_{k=1}^{N_i} m_k v_k^2 \tag{2}$$

where, N_i is number of atoms in ith slab. Furthermore, calculated temperature for each slab T_i is averaged over pre-defined time interval to get a smooth temperature profile. To get the better statistics, the temperature profile could be further blocked averaged over several blocks. At last, the temperature gradient is calculated by the slope of resulting temperature profile.

Similarly, heat flux per unit area, $Q/A\Delta t$ is calculated as follows

$$\frac{Q}{A\Delta t} = \frac{1}{A\Delta t}\left\langle \frac{1}{2}\sum_{k=1}^{N_B} m_k\left(v_k^2 - \mathrm{vp}_k^2\right)\right\rangle \tag{3}$$

where vp_k and v_k are the velocities of the atoms before and after rescaling to desired temperature, respectively. N_B is the number of atoms in the boundary layers. Once the temperature gradient and the heat flux are known, the thermal conductivity is calculated using Eq. (1).

2.2. Formalism of thermal conductivity based on Green-Kubo approach (EMD)

Equilibrium molecular dynamics simulations using Green-Kubo (GK) approach [13] are often used to calculate several transport properties. This approach is based on fluctuation–dissipation theorem and relates the fluctuation properties of a thermodynamic system to its linear response properties. In other words, it provides a pathway to relate out-of equilibrium properties (transport coefficients) with fluctuations in equilibrium properties. The transport coefficients are evaluated by integrating time autocorrelation functions of microscopic fluxes of equilibrium properties. Few of such examples include diffusion coefficient, thermal conductivity, electrical conductivity, viscosity, etc. In particular, the thermal conductivity λ, is calculated by integrating time autocorrelation function of heat flux vector and is given by following equation [25].

$$\lambda = \frac{1}{k_B T^2 V}\int_0^\infty \langle \mathbf{J}(t)\cdot\mathbf{J}(0)\rangle \mathrm{d}t \tag{4}$$

Here $\mathbf{J}(t)$ is the heat flux vector at time t. In addition, V and T represent the volume and temperature of the system, respectively, while k_B is Boltzmann constant. In terms of molecular dynamics entities, $\mathbf{J}(t)$ is written as:

$$\mathbf{J}(t) = \frac{\mathrm{d}}{\mathrm{d}t}\sum_{i=1}^{N}\mathbf{r}_i E_i \tag{5a}$$

where

$$E_i = \frac{1}{2}m_i\mathbf{v}_i^2 + \frac{1}{2}\sum_{j\neq i}^{N}u(r_{ij}) \tag{5b}$$

Here, m_i and $\mathbf{v}_i$ represent mass and velocity of atom i. $u(r_{ij})$ is the total potential energy of atom i whereas r_{ij} is the distance between atom i and j. In most cases, an analytic form of Eq. (5a) is used to evaluate $\mathbf{J}(t)$ which generally depends upon the form of interaction potential $u(r_{ij})$ employed in the simulations. In our case, we have used 12–6 Lennard Jones potential for non-bonded van der Waals interactions along with Ewald summation for electrostatic interactions. In such a case, the final expression for microscopic heat current vector $\mathbf{J}(t)$ sum becomes:

$$\mathbf{J}(t) = \frac{1}{2}\sum_{i=1}^{N}\left[m_i v_i^2 + \sum_{j\neq i}^{N}u(r_{ij})\right]\mathbf{v}_i + \frac{1}{2}\sum_{i=1}^{N}\sum_{j\neq i}^{N}(\mathbf{r}_{ij}\mathbf{F}_{ij}^{R})\cdot\mathbf{v}_i + \frac{1}{2}\sum_{i=1}^{N}\sum_{j=1}^{N}v_i\cdot\mathbf{S}_{ij} \tag{6}$$

In Eq. (6), $\mathbf{F}_{ij}$ represents the short range van der Waals force and real part of Ewald–coulomb force (calculated within prescribed cutoff distance). In addition, it also includes forces due to bonded interaction terms such as bond stretching, angle bending, etc. These forces are computed in real space. On the other hand, tensor S is evaluated in Fourier space. This tensor represents the forces due to electrostatic interactions beyond the cutoff distance. The elements of tensor S are written as [26]

$$\mathbf{S}_{ij}^{\alpha\beta} = \frac{4\pi}{V}\sum_{k\neq 0}^{\infty}B_{\alpha\beta}\frac{1}{k^2}\,e^{-k^2/4R_C^2}Z_iZ_j\cos(\mathbf{k}\cdot\mathbf{r}_{ij}) \tag{7a}$$

$$B_{\alpha\beta} = \delta_{\alpha\beta} - \frac{2|\mathbf{k}_\alpha||\mathbf{k}_\beta|}{|\mathbf{k}|^2} - \frac{|\mathbf{k}_\alpha||\mathbf{k}_\beta|}{2R_C^2} \tag{7b}$$

where α and β denote the directions in reciprocal space, $\mathbf{k}$ represents reciprocal vector, R_C represents Ewald parameter while i and j are atom indices. In addition, Z_i denotes the charge on atom i. The detailed discussion for the inclusion of tensor $\mathbf{S}$ in heat current vector has already been reported in literature previously [27]. Here it is sufficient to say that it is introduced to avoid divergences arising from the long range columbic interactions and takes care of forces due to long range Ewald interactions in Fourier space [28]. The justification to use relatively slower Ewald technique (as compared to faster PPPM technique) to capture the long range interactions efficiently is well documented in literature [27,28] and the references therein.

3. Model protocol and simulation details

The systems studied in current study consist of epoxy resin EPON-862 (di-glycidyl ether of bisphenol F), curing agent-W also known as DETDA (diethylene toluene diamine), and their crosslinked polymer. The epoxy resin, crosslinking agent along with their crosslinking reaction is shown in Fig. 1. For all simulations presented in this study, CVFF (Consistent Valance Force Field) potential [29] was used for bonded as well as non-bonded interactions. This force-field successfully predicted accurate thermodynamic properties of interest for our system of interest [23].

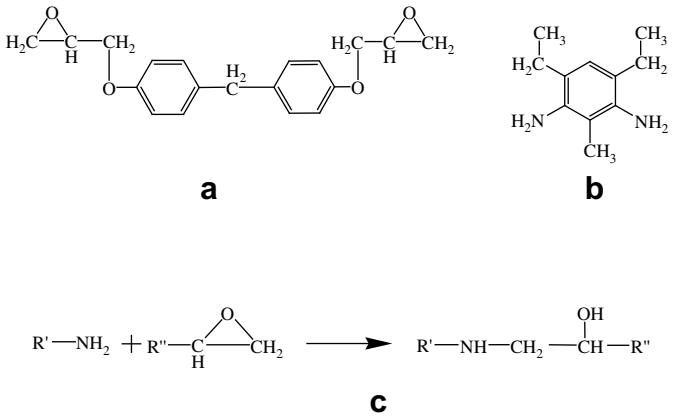

Fig. 1. Molecular structure of (a) EPON-862; (b) DETDA; (c) Crosslinking reaction.

In addition, for NEMD simulations, the long range electrostatic interactions were modeled using PPPM technique [30]. However, since the heat flux Eqs. (6, 7a and 7b) use Ewald summation [31] to calculate electrostatic contributions, the relatively slower Ewald summation technique was employed for long range electrostatic interactions for EMD simulations. All simulations were performed using open source LAMMPS (Large-scale Atomic/Molecular Massively Parallel Simulator) software provided by Sandia National Laboratories [32].

The initial configurations for both DETDA and EPON-862 were modeled using Material Studio® [33]. The crosslinked polymer was subsequently created using a procedure developed by us earlier [23]. As the current article primarily focuses on thermal transport, interested readers are referred to Ref. [23] for detailed crosslinking procedure. Here, we would like to mention that we were able to build a crosslinked network with relaxed structure with calculated thermodynamic and structural properties consistent with experimental data. The system specifics, including no. of atoms, no. of molecules, equilibrated dimensions, etc. for each studied system are tabulated in Table 1. The crosslinked systems under current investigation were 90% crosslinked which corresponds to on average ~3.6 Epon molecules being connected to each DETDA molecule, which has a crosslinking functionality of 4.

At first, all three systems (un-crosslinked epoxy resin, curing agent and crosslinked polymer) were minimized using conjugate gradient method to remove possible overlaps between atoms. Thereafter, constant volume (NVT) and constant pressure (NPT) simulations were run to equilibrate the temperature and density, respectively. The system size dimensions of the resulting equilibrated densities at room temperature (300 K) are also listed in

Table 1
System specifications.

System	Equilibrium MD		Non-equilibrium MD	
	No. of atoms (molecules)	Dimensions (Å^3)	No. of atoms (molecules)	Dimensions (Å^3)
DETDA	9920 (320)	46.5 × 46.5 × 46.5	19840 (640)	23.3 × 23 × 373.3
EPON	4300 (100)	35.9 × 35.9 × 35.9	43000 (1000)	35.9 × 35.9 × 359.9
Crosslinked system[a]	7488 (128, 64)	42.6 × 42.6 × 42.6 (90.0)[b]	14976 (256, 128)	21.4 × 21.4 × 337.3 (90.0)
	14,976 (256, 128)	53.6 × 53.6 × 53.6 (87.5)[b]		

[a] For the crosslinked system, stoichiometric ratio of EPON-862 and DETDA were used. Please refer to reference 23 for further details regarding crosslinking procedure.
[b] The numbers in () signify crosslinking %.

Table 1. Once the initial equilibrated system was achieved, a series of equilibrium molecular dynamics and non-equilibrium molecular dynamics simulations were performed at room temperature.

For equilibrium molecular dynamics runs, after prior equilibration, a constant NVE simulation was performed for 100 ps to get the equilibrated structure in micro-canonical ensemble. Once, the system got equilibrated, further constant energy (NVE) simulations were performed on the newly equilibrated system for data collection for 1.6 ns, where data were collected at 0.01 ps for the calculation of heat current vector and its subsequent analysis.

For non-equilibrium simulations, the elongated slab was divided into 100 smaller slabs of equal thickness. In the central part of the system, 4 slabs were treated as hot region while the 2 slabs on each boundary were treated as cold region. The system was set to be periodic in all 3 dimensions. For current simulations, the hot region was kept at 350 K while cold region was kept at 250 K. After the system is equilibrated from prior NPT simulations, the NEMD simulations in micro-canonical ensemble (NVE) were run for about 1 ns in order to achieve steady-state for heat flow. Once the steady-state was achieved, further simulations for 1.5 ns were run for the data collection at the interval of 0.1 ps for further analysis.

4. Results and discussion

4.1. Non-equilibrium MD: thermal conductivity

For Fourier Law to be applicable to NEMD simulations, there should exist a local thermal equilibrium within the slab [34]. This was confirmed by verifying that the velocity distribution followed the Maxwell–Boltzmann curve in thermostated as well as un-thermostated region. The heat flux and temperature gradient were calculated for all systems being studied, namely, EPON-862, DETDA and the crosslinked polymer. Fig. 2 shows the input (energy put in hot region) and output (energy taken off from cold region) energies as the function of simulation time in a cumulative manner. When the steady-state of the system is reached, the slope of both curves (heat flux) should become constant and equal. Looking at the figure, it is safe to assume that steady-state has been reached for all systems around 1.2 ns. After steady-state system was reached, the heat flux per unit time across the cross-section was calculated from the slope of each curve using least square fitting method and is listed in Table 2.

Table 2
Calculated thermal conductivity using molecular dynamics simulations.

System studied	Heat flux (kcal/mol-Å^2-ps)	Temperature gradient (K/Å)	Thermal conductivities (W/m-K)	
			Non-equilibrium approach	Equilibrium approach
DETDA	3.08×10^{-3}	0.53	0.205 ± 0.003	0.272 ± 0.036
EPON-862	3.08×10^{-3}	0.55	0.211 ± 0.003	0.251 ± 0.041
Crosslinked system	5.12×10^{-3}	0.60	0.302 ± 0.005	0.310 ± 0.048

Along the same lines, the resultant temperature gradient due to steady-state heat flux is plotted in Fig. 3. As mentioned before, the system was divided into 100 slabs or layers. The temperature of each layer was calculated using 1000 samples stored at every 0.1 ps for 100 ps. The temperature was further block averaged over 13 such 100 ps time blocks, followed by averaging over both temperature gradients (from hot thermostated centre slabs). From the figure, it is quite clear that the temperature change across the slab in the un-thermostated zone is linear for all 3 systems. The slope, i.e., temperature gradient was calculated by fitting the central portion of un-thermostated zone to avoid any boundary effects using least square method. The values of the temperature gradient for all 3 studied systems are also listed in Table 2.

Thereafter, the thermal conductivity for all three systems was calculated using Eq. (1) from the values listed in Table 2. The thermal conductivities of DETDA, EPON-862 and their crosslinked network were found to be 0.20, 0.21 and 0.30 W/m-K, respectively. Although, we could not find any reported experimental values of thermal conductivities of DETDA and un-crosslinked EPON-862, the reported value for crosslinked epoxy network is between 0.2 and 0.3 W/m-K [35]. The calculated thermal conductivity is therefore in good agreement with experimental findings and we have shown that NEMD simulations can successfully predict thermal properties of disordered or amorphous systems.

Here, it is worth mentioning that although the current simulations did not explicitly study the effect of frequency of velocity update and the thickness of the controlled (hot and cold) region on the thermal conductivity, these variables should not make any significant difference in the values of predicted thermal conductivity. The significance of such variables has been discussed in literature [34] where the authors did not find any noticeable

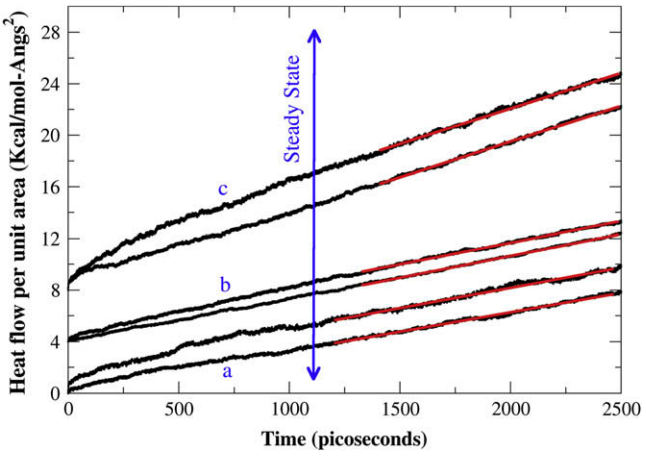

Fig. 2. Heat flux as a function of time. (a) DETDA; (b) EPON-862; (c) crosslinked network. The plots for (b) and (c) are shifted by 4 and 8 kcal/mol-Å^2, respectively, for the sake of clarity. For each system, the upper dataset represents the heat put into the high temperature region while the lower dataset represent the heat taken off from the low temperature region.

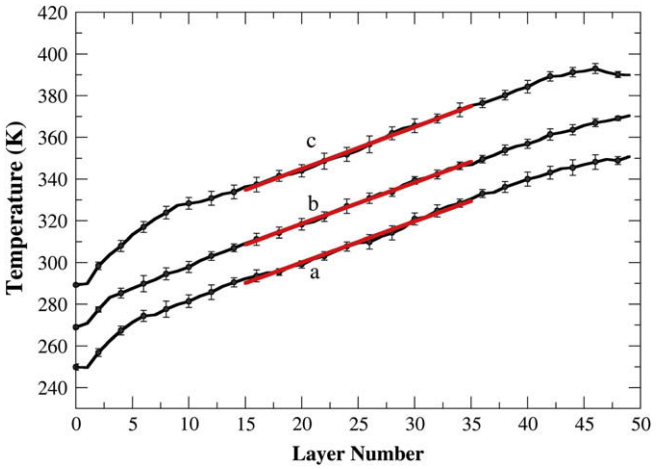

Fig. 3. Temperature profile across slab for: (a) DETDA; (b) EPON-862; (c) crosslinked network; the plots for (b) and (c) are shifted by 20 K and 40 K respectively for the sake of clarity.

change in the values of thermal conductivity as the function of thermostated slab thickness or frequency of velocity update.

4.2. Equilibrium MD: thermal conductivity

Fig. 4 shows the normalized heat flux autocorrelation function and thermal conductivity for all studied systems (refer to Eqs. (4 and 6) in Section 2.2). The results were averaged over three orthogonal directions to get better statistics as they were found to be isotropic in nature for all cases. Fig. 4A shows oscillatory autocorrelation function which decays down to zero around ~2–3 ps for all the three systems.

Fig. 4B shows the plot of thermal conductivity as a function of time, as evaluated from integrating the heat flux autocorrelation function. For all cases, we find that the thermal conductivity first increases, then decreases and becomes constant at longer times when the autocorrelation function decays down to zero. Such a trend in thermal conductivity has been previously observed for oscillatory decaying heat flux autocorrelation function [36]. The high frequency oscillations in heat flux ACF are attributed to optical phonons [37]. The thermal conductivities for DETDA, EPON-862 and the crosslinked network were calculated to be 0.27, 0.25 and 0.31 W/m-K (Table 2). The standard deviation associated with the thermal conductivity values was found to be quite significant and is listed in Table 2 as well. On comparing results from equilibrium and non-equilibrium molecular dynamics simulations, we find a good agreement between both the approaches. However, the results from EMD simulations were found to be slightly higher than those from NEMD simulations for all cases. Comparison of thermal conductivity calculations using two approaches has been reported previously by other groups as well [38]. Although we did not study size effect for NEMD simulations due to computational limitations, we performed an EMD simulation for crosslinked network for a system twice as big as the previous system with ~15 000 atoms (Table 1). The estimated thermal conductivity value was found to be ~0.32 W/m-K, in excellent agreement with the smaller crosslinked system providing us with sufficient confidence that studied system sizes for EMD simulations were large enough for the estimation of thermal conductivity. Additionally, scattering from the heat source and sink is also expected to contribute to thermal resistivity thus lowering the thermal conductivity in the case of NEMD simulations.

4.3. Power spectrum analysis

The power spectrum presents the partial vibrational density of states for each atom and provides an understanding of the energy storage in different parts of the molecule [36]. The partial vibrational density of states (PVDOS) is calculated from real part of Fourier transform of velocity autocorrelation function (ACF) can be written as [39]

$$D_{p,\beta}(\omega) = c_\beta \int_0^\tau \Gamma_\beta(t)\cos(\omega t)\mathbf{d}t \tag{8a}$$

where,

$$\Gamma_\beta(t) = \sum_i^{N_\beta}\left\langle \mathbf{u}_{i\beta}(t)\cdot\mathbf{u}_{i\beta}(0)\right\rangle \Big/ \sum_i^{N_\beta}\left\langle \mathbf{u}_{i\beta}(0)\cdot\mathbf{u}_{i\beta}(0)\right\rangle \tag{8b}$$

Here, $D_{p,\beta}(\omega)$ and $\Gamma(\omega)$ denote the PVDOS and the normalized velocity autocorrelation function for atom type β. c_β denotes the concentration of species of type β. The total vibrational density of states is obtained by summing over the partial density of states.

$$D_p(\omega) = \sum_\beta D_{p,\beta}(\omega) \tag{9}$$

Fig. 5 shows the power spectrum of velocity ACF (PVDOS) of various atomic entities in the crosslinked network. For these calculations, simulations were run for 40 ps where data were stored at each 1 fs timestep. The power spectrum was evaluated from averaged velocity ACF over *X*, *Y* and *Z* directions as ACFs were found to be isotropic in nature for all atomic types. As one can see, the figure presents several peaks for each atomic type. The high frequency peaks represent different vibrations (stretching, bending, etc.) in which corresponding atomic entity is involved. These peaks are often captured by spectroscopic techniques such as IR, Raman spectroscopy, etc. These high frequency vibrations in

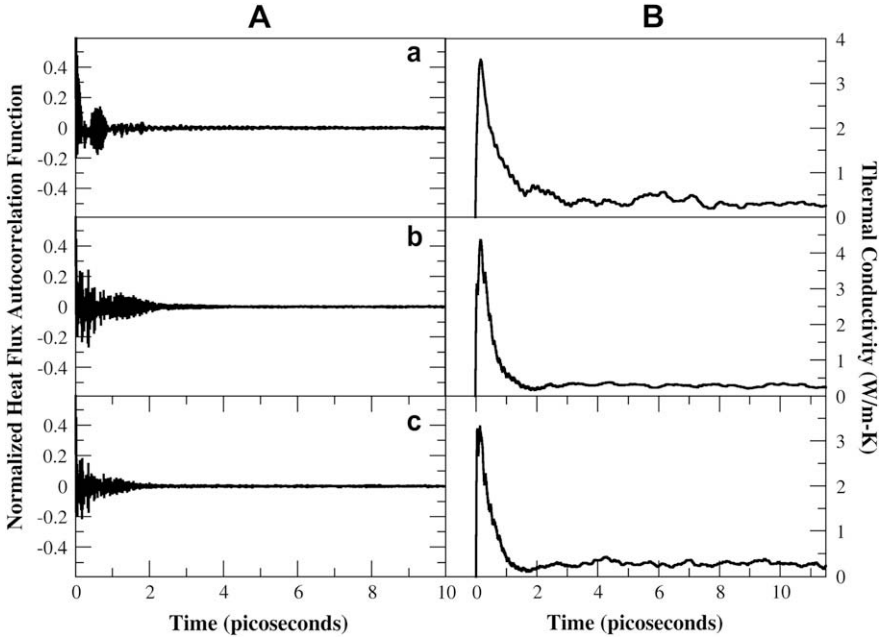

Fig. 4. Normalized heat flux autocorrelation function and resultant thermal conductivities for: (a) DETDA; (b) EPON-862; (c) crosslinked network.

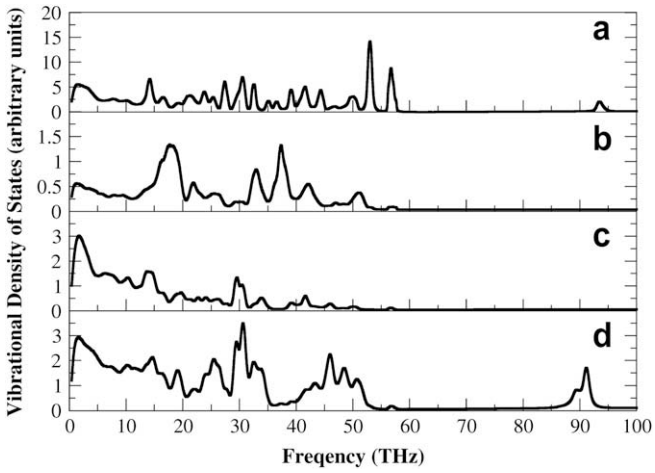

Fig. 5. Vibrational density of states for various atomic entities of crosslinked network as a function of frequency: (a) sp^2 benzene carbon; (b) amine nitrogen; (c) ether and hydroxyl oxygen; and (d) sp^3 carbon in methyl and methylene groups.

polymeric glasses are known to be rarely involved in thermal transport as these modes are localized with negligible thermal diffusivity [22]. The figure also presents a broad low frequency peak which is present for all the atomic entities. These peaks are better depicted in Fig. 6. Generally, these peaks occur below the low frequency limit of IR spectroscopy (~14 THz) and are associated with low frequency modes of vibrations, known to be significant for thermal conduction due to their non-zero thermal diffusivity [22]. For our system, we see one such broad peak, present in power spectra of all atomic entities. The similar position of the peak in all atomic types suggests that significant number of atoms are perhaps collectively involved in such low frequency vibrations. The broadness of the peak over several THz suggests a possible distribution of relaxation times with different overlapping low frequency vibrational modes. Recently, McGaughey et al. did a thermal conductivity analysis of metal organic framework (MOF-5) crystal [36]. Unlike the present case where we observe only one broad peak, the power spectrum analysis by McGaughey et al. shows several sharp peaks in the low frequency vibrational regime (acoustic region), suggesting that these low frequency modes are separated in frequency regime in crystal framework. Based on this observation, the broad nature of the low frequency peak can be attributed to the amorphous nature of our polymer network system as also observed recently by Shenogin et al. [22].

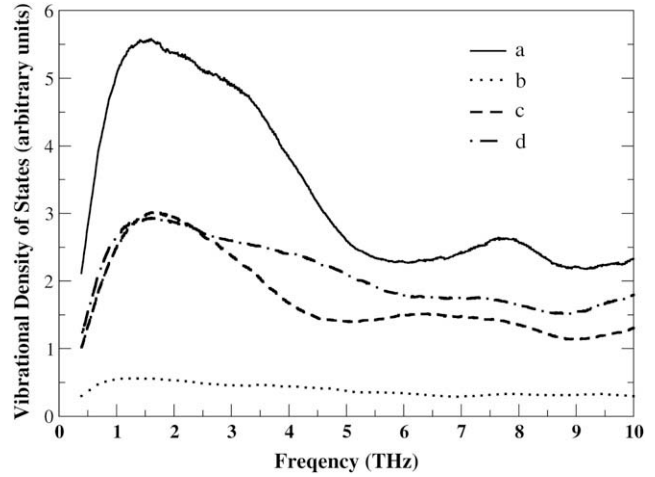

Fig. 6. Low frequency power spectra of velocity autocorrelation function of various atomic entities of crosslinked network. (a) sp^2 benzene carbon; (b) amine nitrogen; (c) ether and hydroxyl oxygen; and (d) sp^3 carbon in methyl and methylene groups.

4.4. Pair contribution analysis

In addition to the thermal conductivity estimation, it should also be interesting and insightful to study and analyze its various convective and virial contributions separately, calculated from equilibrium MD simulations. From Eq. (6), (as discussed in Section 2.2), we observe that heat flux vector indeed comprises of several terms. These terms are associated with (a) convective terms (kinetic energy, van der Waals potential energy and electrostatic energy); and (b) virial terms (forces due to van der Waals interactions, electrostatic interactions and bonded interactions).

In order to capture different contributions, correlations between several terms were evaluated separately. These terms are listed below in detail.

a) Convective: kinetic energy interactions
b) Convective: van der Waals potential energy interactions
c) Convective: electrostatic energy interactions
d) Virial: van der Waals forces
e) Virial: short range electrostatic forces (within electrostatic cutoff distance), calculated in real space
f) Virial: long range electrostatic forces, calculated in reciprocal space.
g) Virial: bond stretching forces
h) Virial: angle bending forces.

For example, in order to evaluate thermal conductivity due to convective terms (kinetic and potential energy contributions) only, we summed up the terms associated with a) and b), while ignoring other terms. For our analysis, we represent the contribution by index "1" and lack of contribution by index "0". To clarify further, description "10000000" suggests that only kinetic energy convective contribution is taken into consideration while ignoring others for thermal conductivity estimation. We believe that such an approach should also take care of possible crossterms implicitly.

Several of such contributions are listed in Table 3 along with the resultant thermal conductivities. The most important findings that emerge from this analysis are presented in form of pie-charts in Fig. 7 and are discussed below.

a) Plot 7a shows the distribution of overall thermal conductivity in terms of total virial and convective terms. The plot suggests that the contributions from virial terms have a dominating effect than convective terms towards total thermal conductivity. Such a behavior has also been reported earlier for ionic systems [31]. In the present case, however, the convective contributions (kinetic, van der Waals and electrostatic interactions) although low are significant. In addition, the cross-correlation between convective and virial terms was found to be insignificant.

Table 3
Thermal conductivity values for different heat flux contributions.

	Contribution description	λ (W/m-K)	Standard deviation
1	00000011	0.000[a]	0.000
2	11100000	0.026	0.002
3	00010000	0.270	0.046
4	00011000	0.286	0.046
5	00011100	0.287	0.045
6	11011000	0.309	0.047
7	11111111	0.315	0.049
8	11111100	0.317	0.049
9	11111000	0.317	0.049

[a] The thermal conductivity was estimated to be 0 within 3 decimal places.

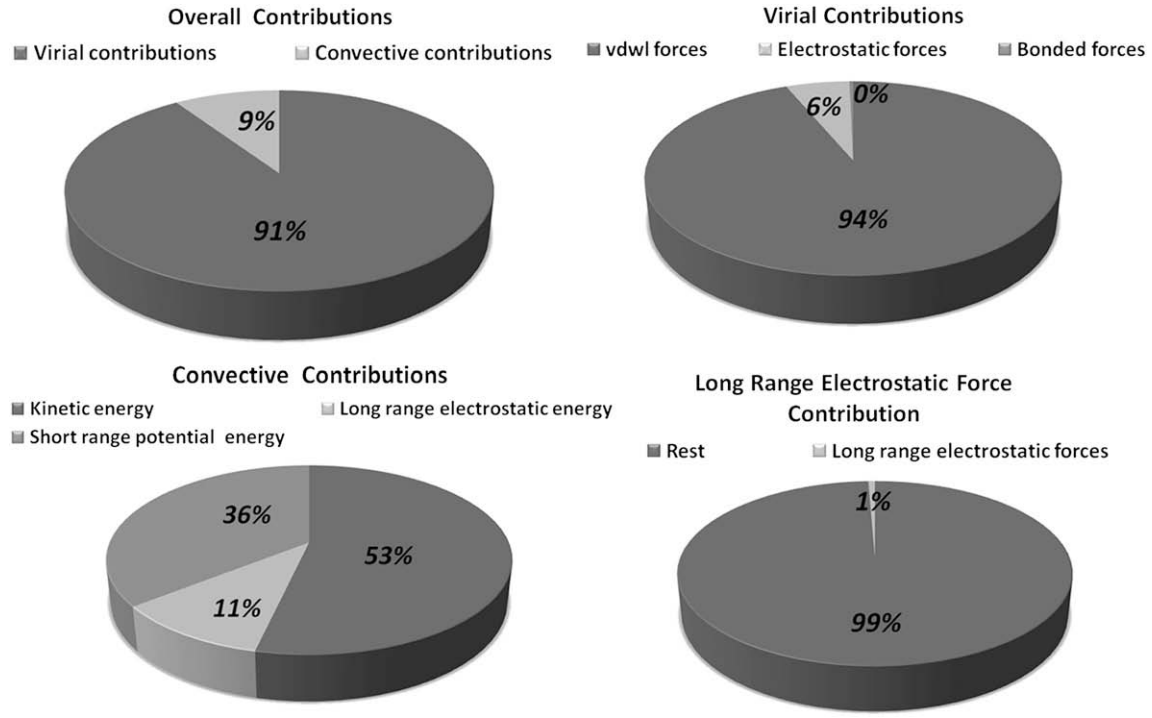

Fig. 7. Pie-chart of thermal conductivity contributions from various heat components.

b) Plot 7b shows the distribution of various virial contributions. The virial contribution from the forces due to van der Waals interactions is the most dominating among different virial contributions to thermal conductivity. The plot also shows that virial contributions from bond stretching and angle bending terms are negligible.
c) Plot 7c shows the distribution of various convective terms and suggests that kinetic energy and short range potential energy dominate the contribution while the contribution from long range electrostatic potential energy is low.
d) Plot 7d shows the contributions from long range electrostatic forces to overall thermal conductivity and suggests that these contributions are negligible. This suggests that such contributions can be neglected while doing thermal analysis for organic, neutral polymeric systems.

In summary, the aforementioned analysis suggests that the dominant modes of heat transport for disordered amorphous polymeric materials are due to van der Waals interactions and their corresponding forces. As these interactions result in anharmonic modes of vibrations, our results are in agreement with recent study which suggests that anharmonic interactions contribute significantly towards thermal conductivity in polymeric glasses [22]. It has been suggested in literature that in polymeric glasses, a large fraction of the vibrational modes (especially high frequency vibrational modes) is localized with negligible thermal diffusivity [22]. Keeping that in mind, contributions from these vibrational modes towards thermal conductivity are expected to be insignificant. This is also in agreement with our results which suggest negligible contribution of bonded interactions towards thermal conductivity.

5. Summary and conclusions

This article presents one of the first atomistic molecular dynamics studies of heat transport in crosslinked polymers (epoxy polymers). Both equilibrium and non-equilibrium molecular dynamics simulations were used to estimate the thermal conductivity of epoxy networks at room temperature. Given quite diverse experimental conditions such as curing time, temperature, humidity, etc. for building epoxy thermosets, the calculated thermal conductivity, λ is in good agreement with experimental values. The broad distribution of low frequency vibrational modes as calculated from partial vibrational density of states is indicative of overlapping distribution of low frequency vibrational modes and the amorphous nature of the polymer. Furthermore, the analysis from different contributions towards heat flux autocorrelation function suggested that virial contribution from van der Waals interactions dominate the thermal conductivity with negligible contributions from bonded and electrostatic interactions. Given the dominant contribution of van der Waals interactions towards thermal conductivity, the higher thermal conductivity of epoxy network (compared to its un-crosslinked counterparts) can be attributed to densification of the network during crosslinking, which enhances neighboring non-bonding interactions.

Acknowledgements

This work was performed under U.S. Air Force Contract No. F33615-030D-5801, 0059. The two lead authors (Varshney and Patnaik) greatly appreciate the financial support in performing this work. The authors are also thankful to Alan J. McGaughey, Sergei Shenogin and Pawel Keblinksi for their helpful discussions during the course of this study.

References

[1] Carslow HS, Jaeger JC. Conduction of heat in solids. 2nd ed. Oxford: Oxford University Press; 1986.
[2] Chung DDL. Applied materials science: applications of engineering materials in structural, electronics, thermal, and other industries. New York: CRC Press; 2001.

[3] May CA, editor. Epoxy resins: chemistry and technology. 2nd ed. New York: CRC Press; 1988.
[4] Sihn S, Ganguli S, Roy AK, Qu L, Dai L. Compos Sci Technol 2008;68(3–4):658.
[5] Baur J, Silverman E. MRS Bull 2007;32(4):328.
[6] Huang H, Liu CH, Wu Y, Fan S. Adv Mater 2005;17(13):1652.
[7] Karpov VG, Parshin DA. Pis'ma Zh Eksp Teor Fiz 1983;38:536.
[8] Jagannathan A, Orbach R, Entin-Wohlman O. Phys Rev B 1989;39(18):13465; Alexander S, Entin-Wohlman O, Orbach R. Phys Rev B 1986;34(4):2726.
[9] Feldman JL, Allen PB. Phys Rev B 1993;48(17):12581; Feldman JL, Kluge MD, Allen PB, Wooten F. Phys Rev B 1993;48(17):12589.
[10] Frenkel D, Smit B. Understanding molecular simulation: from algorithms to applications. 2nd ed. San Diego: Academic Press; 2002.
[11] Gou J, Minaie B, Wang B, Liang Z, Zhang C. Comput Mater Sci 2004;31:225; Fan HB, Yuen MMF. Polymer 2007;48:2174; Wu C, Xu W. Polymer 2006;47:6004.
[12] Heine DR, Grest GS, Lorenz CD, Tsige M, Stevens MJ. Macromolecules 2004;37:3857.
[13] Kubo R, Toda M, Hashitsume N, Saito N. Statistical physics II. Berlin: Springer; 1985.
[14] McGaughey AJH, Kaviany M. Adv Heat Transfer 2006;39:169 [chapter 2].
[15] Maiti A, Mahan GD, Pantelides ST. Solid State Commun 1997;102(7):517.
[16] Kondo N, Yamamoto T, Watanabe K. e-J Surf Sci Nanotech 2006;4:239; Osman MA, Srivastava D. Nanotechnology 2004;12:21; Yao Z, Wang J-S, Li B, Liu G-R. Phys Rev B 2005;71:85417; Noya EG, Srivastava D, Chernozatonskii LA, Menon M. Phys Rev B 2004;70:115416; Che J, Cagin T, Goddard III WA. Nanotechnology 2000;11:65; Moreland JF, Freund JB, Chen G. Microscale Thermophys Eng 2004;8:61; Berber S, Kyon Y-K, Tománek D. Phys Rev Lett 2000;84(20):4163; Bi K, Chen Y, Yeng J, Wang Y. Chem Phys Lett A 2006;350:150.
[17] Osman MA, Srivastava D. Phys Rev B 2005;72:125413.
[18] Kawamura T, Kangawa Y, Kakimoto K. Phys Stat Sol (c) 2006;3(6):1695; Yoon Y, Car R, Srolovitz DJ, Scandolo S. Phys Rev B 2004;70:012302.
[19] Phillpot SR, Schelling PK, Keblinski PJ. Mater Sci 2005;40:3143; Zenghui W, Zhixin L. Appl Therm Eng 2006;26:2063; Feng X-L, Li Z-X, Guo Z-Y. Microscale Thermophys Eng 2003;7:153.
[20] Chantrenne P, Raynaud M, Baillis D, Barrat JL. Microscale Thermophys Eng 2003;7:117.
[21] Terao T, Lussetti E, Muller-Plathe F. Phys Rev E 2007;75:057701.
[22] Shenogin S, Bodapati A, Keblinski P, McGaughey AJH. J Appl Phys 2009; 105:034906.
[23] Varshney V, Patnaik SS, Roy AK, Farmer BL. Macromolecules 2008;41:6837.
[24] Anderson CVDR, Tamma KK. Int J Numer Methods Heat Fluid Flow 2004; 14(1):12.
[25] Evans DJ, Morriss GP. Statistical mechanics of nonequilibrium liquids. 2nd ed. New York: Cambridge University Press; 2008.
[26] Hayes DM. Phys Rev B 1994;49:755.
[27] Motoyama S, Ichikawa Y, Hiwatari YOeA. Phys Rev B 1999;60:292; Bernu B, Vieillefosse P. Phys Rev A 1978;18:2345; Nijboer BRA, De Wette FW. Physica (Utrecht) 1957;23:309.
[28] Galama N, Nieto de Castro CA, Ely JF. J Chem Phys 2004;120(18):8676.
[29] Dauber-Osguthorpe P, Roberts VA, Osguthorpe DJ, Wolff J, Genest M, Hagler AT. Protein Struct Funct Genet 1988;4:31.
[30] Hockney RW, Eastwood JW. Computer simulation using particles. New York: Taylor & Francis Group; 1988.
[31] Bresme F, Hafskjold B, Wold I. J Phys Chem 1996;100:1879.
[32] Plimpton SJ. J Comput Phys:1. Code available at: http://lammps.sandia.gov, 1995;117.
[33] Accelrys Inc, San Diego, CA, (module: Amorphous Builder).
[34] Chantrenne P, Barrat J-L. J Heat Transfer 2004;126:577.
[35] Ganguli S, Roy AK, Anderson DP. Carbon 2008;46(5):806.
[36] Huang BL, McGaughey AJH, Kaviany M. Int J Heat Mass Transfer 2007;50:393.
[37] McGaughey AJH, Kaviany M. Int J Heat Mass Transfer 2007;47:1799.
[38] Schelling PK, Phillpot SR, Keblinski P. Phys Rev B 2002;65:144306.
[39] Loong C-K, Vashishta P, Kalia RK, Jin W, Degani MH, Hinks DG, et al. Phys Rev B 1992;45:8052.